Lab on a Chip

Multilevel Fluidic Flow Control in a Rotationally-driven Polyester Film Microdevice Created Using Laser Print and Cut

Journal:	*Lab on a Chip*
Manuscript ID	LC-ART-10-2015-001332.R1
Article Type:	Paper
Date Submitted by the Author:	29-Nov-2015

Complete List of Authors:	Ouyang, Yiwen; University of Virginia, Department of Chemistry Li, Jingyi; University of Virginia, Chemistry Phaneuf, Christopher; Georgia Institute of Technology, Mechanical Engineering Riehl, Paul; University of Virginia, Chemistry Forest, Craig; Georgia Institute of Technology, Mehanical Engineering Begley, Matthew; University of California,Santa Barbara, College of Engineering Haverstick, Doris; University of Virginia Health Science Center, Pathology Landers, James; University of Virginia, Department of Chemistry; University of Virginia, Mechanical Engineering; University of Virginia Health Science Center, Pathology

Multilevel Fluidic Flow Control in a Rotationally-driven Polyester Film Microdevice Created Using Laser Print, Cut and Laminate

Yiwen Ouyang[a], Jingyi Li[a], Christopher Phaneuf[b], Paul S. Riehl[a], Craig Forest[b], Matthew Begley[c], Doris M. Haverstick[d], and James P. Landers[a,d,e]

[a]Department of Chemistry, McCormick Road, University of Virginia, Charlottesville, VA 22904
[b]Mechanical Engineering, 315 Ferst Drive, Georgia Institute of Technology, Atlanta, GA 30332-0363
[c]Department of Mechanical Engineering & Materials Department, University of California Santa Barbara, Santa Barbara, CA, 93106Address here.
[d]Department of Pathology, University of Virginia Health Science Center, Charlottesville, VA 22908
[e]Department of Mechanical Engineering, University of Virginia, Engineer's Way, Charlottesville, VA 22904

A simple and cost-effective polyester toner microchip was fabricated to provide fluid handling on a centrifugal platform.

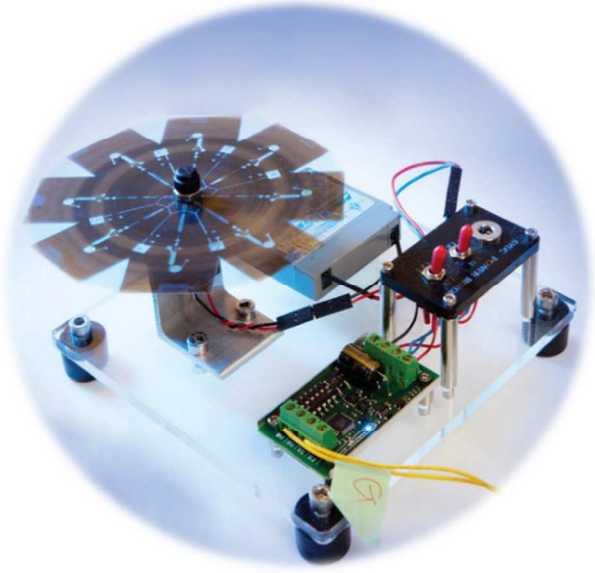

Cite this: DOI: 10.1039/c0xx00000x

www.rsc.org/xxxxxx

ARTICLE TYPE

Multilevel Fluidic Flow Control in a Rotationally-driven Polyester Film Microdevice Created Using Laser Print, Cut and Laminate

Yiwen Ouyang[a], Jingyi Li[a], Christopher Phaneuf[b], Paul S. Riehl[a], Craig Forest[b], Matthew Begley[c], Doris M. Haverstick[d], and James P. Landers[a,d,e]

Received (in XXX, XXX) Xth XXXXXXXXX 20XX, Accepted Xth XXXXXXXXX 20XX
DOI: 10.1039/b000000x

This paper presents a simple and cost-effective polyester toner microchip fabricated with laser print and cut lithography (PCL) to use with a battery-powered centrifugal platform for fluid handling. The combination of the PCL microfluidic disc and centrifugal platform: (1) allows parallel aliquoting of two different reagents of four different volumes ranging from nL to μL with an accuracy comparable to a piston-driven air pipette; (2) incorporates a reciprocating mixing unit driven by a surface-tension pump for further dilution of reagents, and (3) is amenable to larger scale integration of assay multiplexing (including all valves and mixers) without substantially increasing fabrication cost and time. For a proof of principle, a 10-min colorimetric assay for the quantitation of the protein level in the human blood plasma samples is demonstrated on chip with a limit of detection of ~5 mg/mL and coefficient of variance of ~ 7%.

Introduction

Over the last decade, there has been growing interest in the development of low cost diagnostic microfluidics for broad distribution, which typically implies devices manufactured with direct patterning (e.g. printing) and capillary-driven flows. Paper-based microfluidics are arguably the most prominent example of the shift away from complex surface micromachining methods and pressure-driven flows [1,2], and have been demonstrated for glucose, protein, cholesterosterol and lactate detection/quantitation, as well as nucleic acid extraction [3–6]. While paper-based technologies continue to evolve and will undoubtedly have a deep impact on many diagnostic applications, the inherent challenges to flow control – notably mixity and efficiency in sample/reagent transfer[7] – strongly suggest that alternative technologies are needed for a broad range of applications.

One such technology that holds significant promise is the use of inexpensive polymer films (e.g., transparency slides) in conjunction with laser print lithography (LPL), requiring only a cutter, a conventional laser printer and a laminator[8]. Even inexpensive laser cutters can pattern complex microchannels in a highly automated fashion: the channels are closed by using additional sheets with printer toner patterned around the channel, which achieves bonding when the stack is rolled through a conventional laminator.[9] This approach enables simple inexpensive fabrication of complex networks within a plane. After the initial investment in the laser cutter, laser printer and laminator, even complex devices can be made in minutes for less than two (US) dollars.

These devices can then be used with centrifugal platforms to control flow[10]. In this approach, the entire chip is rotated, with the rotation speed controlling flow rates via inertia. Critically, effective approaches to implement valves have been demonstrated using the above fabrication strategy; patterned toner patches at different gray scales are used to modulate hydrophobicity in the channel and create critical burst pressures above capillary pressures, which are then achieved at a critical rotational speed. In this work, we demonstrate the added ability to achieve dilution in such platforms using a combination of such valves and mixing functionality that is actuated by the oscillations in the perpendicular direction of rotation.

The purpose of the paper is to highlight the ability to integrate a number of fluidic control elements in a microfluidic disc created using LPL fabrication to achieve a basic diagnostic functionality (in this case, protein quantification). The functionality requires fluid metering/ aliquoting and mixing, and thus, represents an effective demonstration of fundamental operations required by a broad range of applications. Microlfuidic features on the PCL microdevice include: (1) an aliquoting microfluidic network compatible with viscous samples; (2) for the first time, a passive, rotation-activated reciprocating mixer was designed and proven to be efficient on **P**oly**e**ster **T**oner (PeT) microchip; (3) a three dimensional network achieved by cutting vias/interconnections between layers to allow for parallel fluidics on different vertical levels of the microchip.

Overview of the Device Design and Operation

A schematic illustration of the device concept is shown in **Figure** 1A and 1B. An overview of the chip assembly is shown

in **Figure** 1C, while details of the device operations are shown in

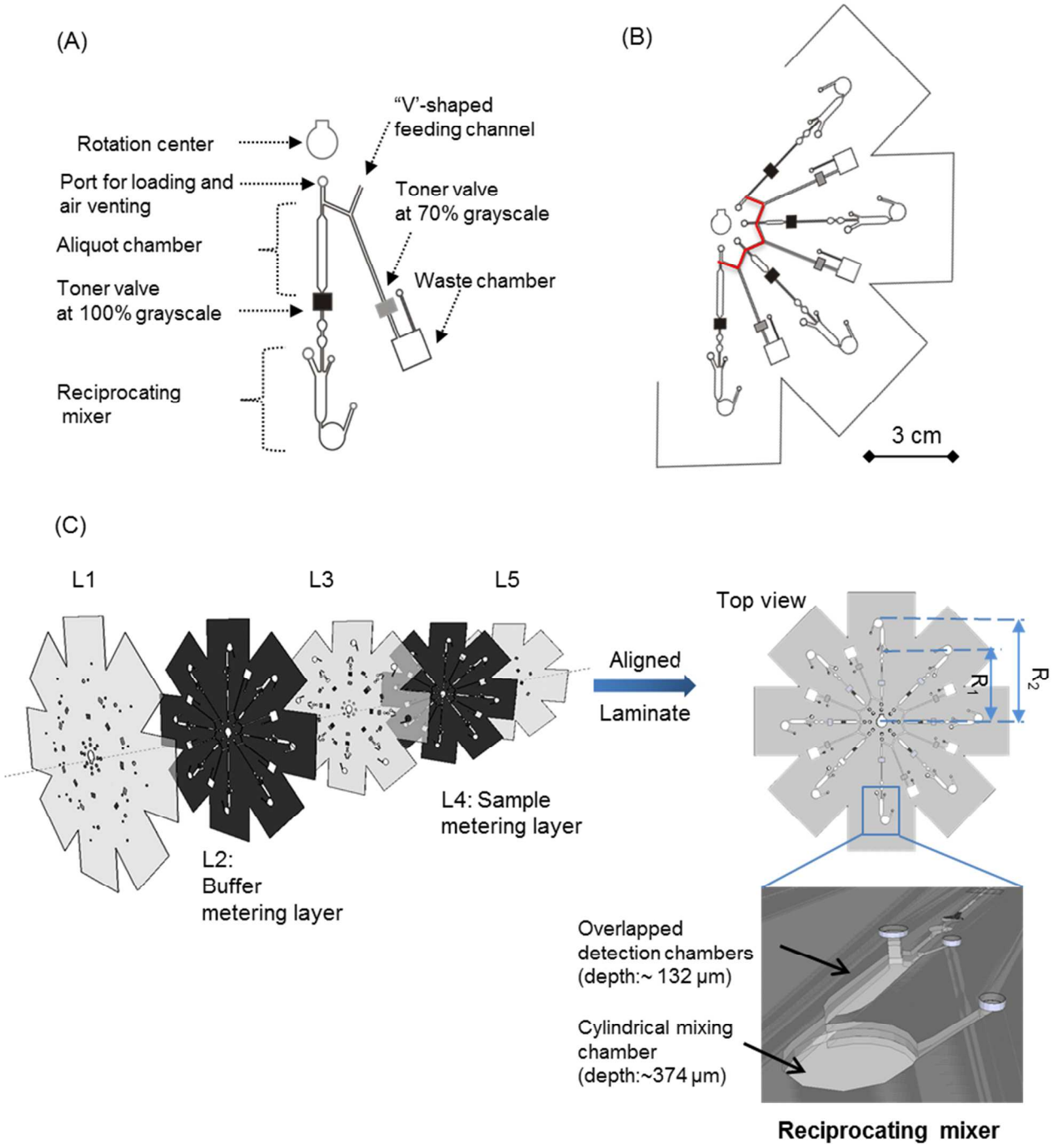

Fig.1 Schematic illustration of the design concept and fabrication process. (A) The design detail of a metering branch on the sample metering layer. (B) Microfluidic network of one single sample aliquot domain on a CD-like dilution microchip for volume splitting. The 'feed channel' is highlighted in red. The design of the buffer aliquot part is similar but with different size of aliquot chambers. (C) Schematic showing assembly of a five-layer CD–like dilution microchip, consisting of transparency films and printer toner with the 3D image shows the detailed view on a single reciprocating passive mixer. The thickness of the microchip is 573 μm.

Cite this: DOI: 10.1039/c0xx00000x

www.rsc.org/xxxxxx

ARTICLE TYPE

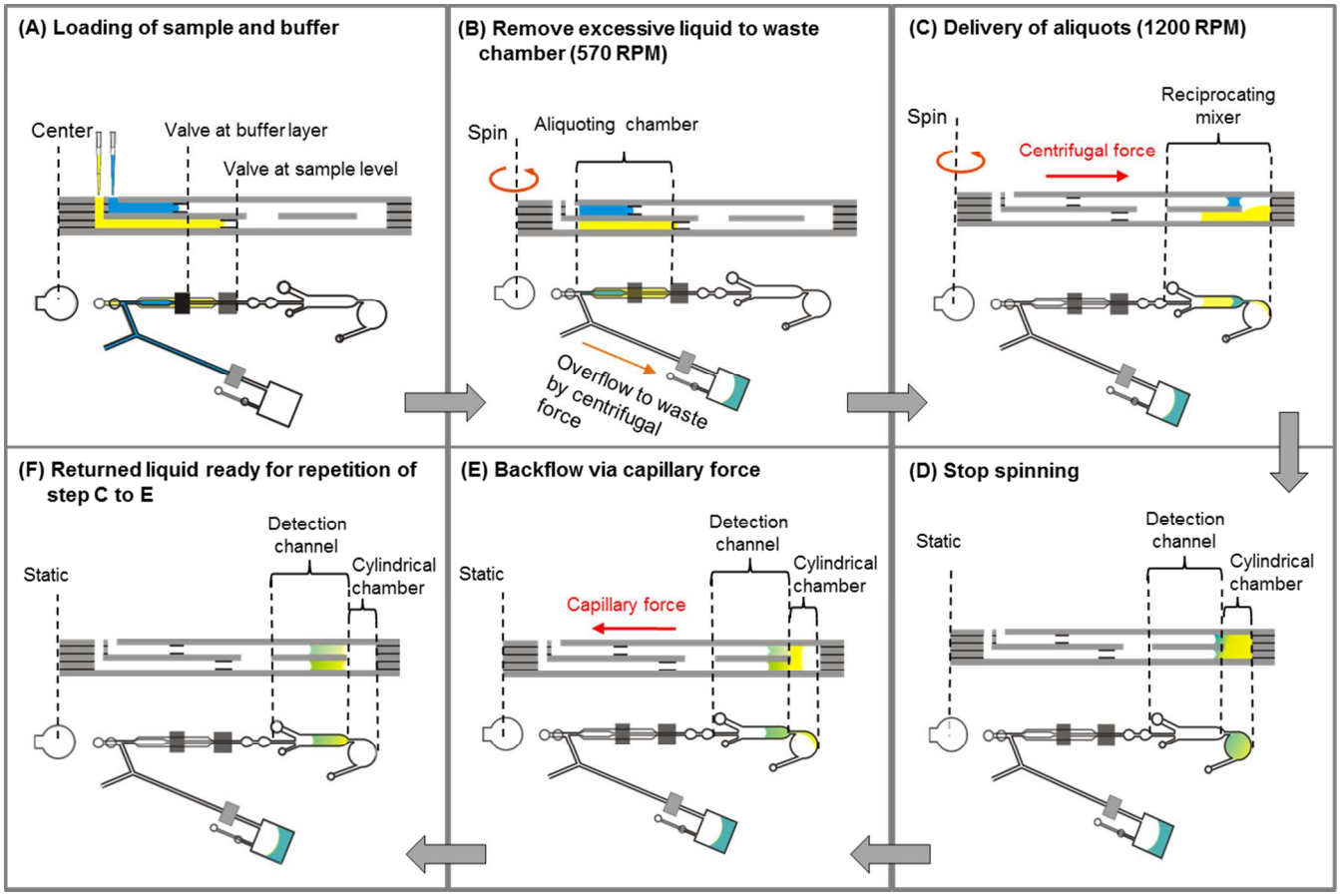

Fig.2: A schematic showing the operation of five-layer PeT microchip for multi-level fluidic handing for the sample dilution from the side-view.

Figure 2. While the sequence of flow patterns is somewhat complex due to the multilevel nature of the microfluidic network, the basic operation of the device can be understood by examining the basic features of the single branch shown in **Figure** 1A, which consists of a feed channel, an aliquot chamber, a reciprocating mixer, a waste chamber and a port at the center which serves either as a reservoir for liquid loading or as an air vent for air to flow depending on the operational stage.

The dark squares in **Figure** 1A represent printed toner patches that act as hydrophobic valves, which permit flow when a critical pressure is generated via centrifugal forces during rotation of the entire chip. The amount of fluid in the aliquot chamber is controlled by patterning different densities of toner in the square patches, which controls the break-through pressure[10]. **Figure** 1B illustrates how multiple branches are included in a single sample aliquoting domain so that parallel operations can be executed. By simply varying the dimensions of aliquot chambers, the aliquot domain can accommodate aliquot volumes ranging from ~250 nL to 2.25 µL. The aliquoting network in the buffer metering level is similar, but has volumes that differ from that of the sample metering level. The volume ratios for the sample metering chamber to the buffer metering chamber (connected to the same mixing domain), are varied to generate four different dilutions ranging from 1.25 to 10 with a final volume of 2.5 µL. There are two identical aliquoting domains on each PCL microfluidic disc.

The sequence of the 'global' operations needed to conduct protein quantitation (described in the final section of this paper) is given in **Figure** 2, which depicts side views of a single branch of the network shown in **Figure** 1A. The operations are as follows:

(A) Undefined sample and buffer volumes (12-14 µL) are loaded into different levels of the network through the ports at the center of the microchip. Due to the hydrophilic nature of the silica-doped transparency film, capillarity drives the sample/reagent into the distribution channel; this automatically primes a series of branched aliquoting chambers and channels led to waste chambers until the hydrophobic barrier is encountered. As a result, the sample and buffer volume loaded into the system is reliable and accurate.

(B) Excess sample and buffer are removed from the loading chambers by spinning at low speed (570 RPM), which is too low to breakthrough in the toner valves (hydrophobic barrier) that separate the aliquoting chamber from the reciprocating mixer, but high enough to mobilize the excessive liquid in the feeding channel to the waste chamber. This is achieved by the use of two toner valves with varied hydrophobicity, facilitated by printing at different grayscales that correspond to different burst pressures. As a result, the liquid remaining in the aliquot chamber is isolated from that in the waste channel by a plug of air in the distribution channel.

(C) The rotation speed is increased to 1200 RPM to force the fluids in sample and buffer levels past the toner valves into the cylindrical mixing chamber of the reciprocating mixer.

(D) Spinning is terminated, which then allows for (E).

(E) Driven by the capillary action, the fluid flows from the mixing chamber back into the split levels of the detection channels that are connected to the mixing chamber.

(F) After the fluid has returned to the split detection channels, the mixing process is repeated by returning to step (C).

Following the *Methods and Materials* section, we describe the operation of the device and demonstrate the precision and accuracy of metering using a combination of hydrophobic valving and other features, rapid mixing using a reciprocating mixer and, finally, full integration of aliquoting and mixing functionalities for parallel dilution, actuated solely by rotation speed control, applied to the direct quantitation the protein in human blood plasma.

Methods and Materials

Chip fabrication

The protocol for the assembly of a five-layer PeT microchip (see Fig. 1C) was modified from that fabrication method for three-layer PeT microchip reported in our previous work[10]. Briefly, the first (L1), third (L3), fifth layer (L5) of the polyester(Pe) transparency film were first selectively patterned by a series of toner patches by a laser printer (HP laserjet 4000) using black toner cartridge (HP C-4127X) to define the hydrophobic barriers, using by a design generated with AutoCAD LT 2004 (Autodesk Inc., San Rafael, CA). For L1 and L5, only the bottom surface and top surface were toner-patterned respectively. The patterned toner arrays on the top and bottom surface of L3 were printed in the mirror image of that on the L1 and L5 respectively. In such manner, the toner patterned on the L1 and top surface of L3 defines the ceiling and the floor of the hydrophobic valves for the buffer metering while the toner patterned patches on the bottom surface of the L3 and on the L5 defines the hydrophobic valves for the sample metering. The L2 and L4 layers were printed with two uniform coating layers of toner on each side.

Following the printing, five layers were ablated by a CO_2 laser system to cut access holes on L1 and L3 to serve as reagent loading reservoirs. Aliquoting microfluidic networks for buffer and sample were ablated into the L2 and L4 respectively. In the mixing region, all the middle layers (L2-L4) were ablated according to the detailed design shown in Fig. 1C. The laser ablation parameters can be found in our previous work[10]. After the ablation, five layers were visually aligned with the assistant of alignment holes and inserted into an in-house modified heated roll laminator (UltraLam 250B) with a temperature of 150 ºC and an estimated speed of 8 mm/ second. During the lamination, the toner coatings on L2 and L4 were melted and bonded to the neighboring layers, while the hydrophobic toner barriers on the L1, L3 and L5 layers was spaced by L2 and L4 layers, thus remained their integrity. The three-layer metering microchips, used in the calibration experiment, were fabricated using the similar procedure without layers L4 and L5. The average thickness of the Pe film is 110 μm and that of the toner layer is 7 μm. Hence, the average thickness of the middle layer, which consists of Pe film with 2 layers of toner on each side, was determined to be 132 μm.

Centrifugal platform

The spinner step used to generate controlled centrifugal force consists of a computer-controlled motor (5:1 MicroMetal Gearmotor HP) which provides a rotational frequency from 200 rpm to 2500 rpm based on the voltage input with an increase interval of ~30 rpm. The motor stops at an input voltage of 2.5 V and spins at full speed in the reverse/forward direction at 0 V/5 V respectively when a chip is attached. The system can be either powered solely by the battery (PS-605W, Power-sonic battery) or be connected to a power adapter which will supply the power in parallel with the battery, in turn charging the battery while it runs. The voltage control utilizes a LabVIEW (National Instruments, Austin, TX, USA) application to define the analogue input to the motor via a data acquisition card (6024-E, National Instruments).

Reagents

All the reagents were purchased from Sigma-Aldrich if not specified otherwise. The blue dye and yellow dye solutions were prepared by dissolving erioglaucine and tartrazine in a 10 mM tris (Fisher Scientific)/1 mM EDTA (TE) buffer at a pH of 7.51 (measured by a Mettler Toledo MP 220 pH meter) to a final concentration of 2.7 mM and 3.7 mM respectively. The green dye solution is a mixture of the blue dye and the yellow dye solution in a ratio of 3:1 (v/v).

The indicator for the colorimetric protein assay was prepared by modifying the recipe in a known procedure[11]: 3.3 mM tetrabromophenol blue (TBPB) (VWR) was first dissolved in the pure ethanol, and then mixed with 250 mM citrate buffer solution (pH=1.8) by 1:1 ratio (v/v). The preparation of the artificial blood plasma buffer was prepared following a procedure described elsewhere[12]. The protein concentration in the artificial blood plasma was adjusted by dissolving different mass of human serum albumin (HSA) in the artificial blood plasma buffer.

Quantification of metering and mixing

To quantitate the metered volume, the three-layer PeT microchip with the metered yellow dye in the serpentine channels was scanned by a desktop scanner (Epson Perfection V100 Photo Scanner) at 1200 dpi and 24 bit color resolution. The pixels which represent the black toner were first discarded by setting a hue-based threshold and the rest of the pixels were processed into

binary with the gray level threshold set by an

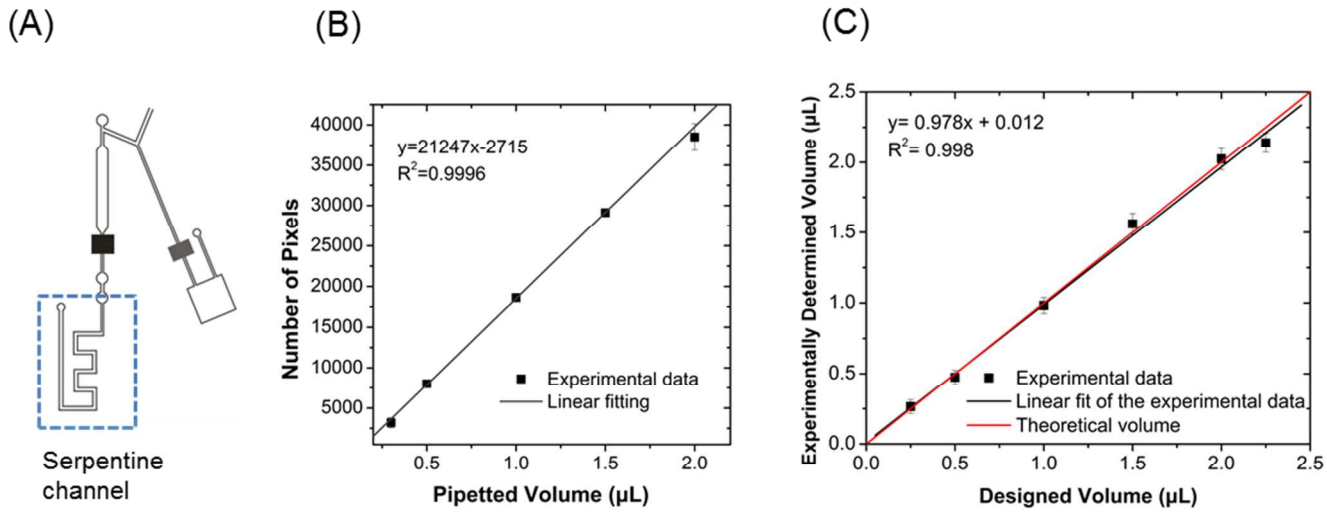

Fig.3: Validation of the metering performance on chip. (A) A design of the serpentine channel that used for measuring the aliquot volume. (B) A calibration curve correlating the pixel number in yellow with the aliquot volume of yellow dye (n=4) in the serpentine channel. (C) Comparison of the empirical volumes on the PeT microchip with the calculated aliquot volumes based on the sample metering design and the buffer metering design (n=4).

isodata algorithm written in *Mathematica* software (*Wolfram Mathematica*, Champaign, IL, USA). After that, the total number of pixels that represent the yellow dyes were quantitated.

The same scanner setting was used to evaluate the mixing performance but with a different isodata algorithm. Artifacts from the black toner was first eliminated by using the same hue-based algorithm. The rest of pixels representing the dyes were converted into a gray-level histogram, representing the full area of the mixing chamber and the standard deviation was calculated. For the analysis of dilution performance and the colorimetric assay, the same algorithm was employed to exclude the artifacts from the black toner and an average hue of the mixing region was calculated based on all the pixels representing the mixtures.

Results and Discussion

The results describing the development of this protein quantification microchip are divided into four sub-sections. The metering and reciprocating mixing functionality will be presented in the first two sections, while the remaining two sections will discuss the integration of the metering and mixing to achieve dilution and an exemplary application of diluting the serum sample for the on-chip protein quantitation.

Aliquoting performance

Figure 3 illustrates the efficacy of the metering strategy that was described earlier. In these experiments, the mixing chamber in the principle device shown in **Figure** 1A was replaced with a serpentine channel (see **Figure** 3A) that could be exploited to accurately quantify through the image analysis, the volume of fluid that 'breaks through' the toner valve, while excess fluid is driven to a waste chamber. Yellow dye was used to mimic the sample for better visualization in the image analysis. **Figure** 3B shows the calibration curve that relates the pixel number of yellow to the volume of yellow dye in the serpentine output channel loaded by routine pipetting. In this manner, the actual volume of aliquoted yellow dye transferred from the metering chamber to the serpentine channel can be determined by plugging the measured yellow pixel number into the calibration curve. The coefficient of variance (C.V.) associated with the pipetted volumes determined through the image analysis of the serpentine channel (e.g., 19.8% for 250 nL, 1.4% for 1.5 μL, 5% for 2 μL) was in general agreement with the pipetting coefficient of variance provided by the manufacturer (12% for 250 nL, 2.5% for 1.25 μL and 1.4% for 2.5μL)[13]. We believe that this can be attributed to the inter-channel depth variation and uncertainty in determining the rough channel edge and the geometry of the meniscus at end of the liquid plug. Nevertheless, the value for coefficient of determination (R^2) confirmed that the liquid volume in the serpentine channel can be proportionally derived from pixel number. Since most analytical techniques use relative measurements, the optical detection method is applicable to validate our aliquot microfluidic network on the PeT microchip with the proposed application. **Figure** 3C shows the excellent correlation between the measured volume and the 'theoretical volume', which is calculated based on nominal channel dimensions (the designed dimensions). Standard deviation for sub-microliter aliquot volumes below 1 μL is ±48-56 nL, while aliquot volumes between 1.5 μL and 2.25 μL had standard deviations ranging from 58-78 nL.

Cite this: DOI: 10.1039/c0xx00000x

www.rsc.org/xxxxxx

ARTICLE TYPE

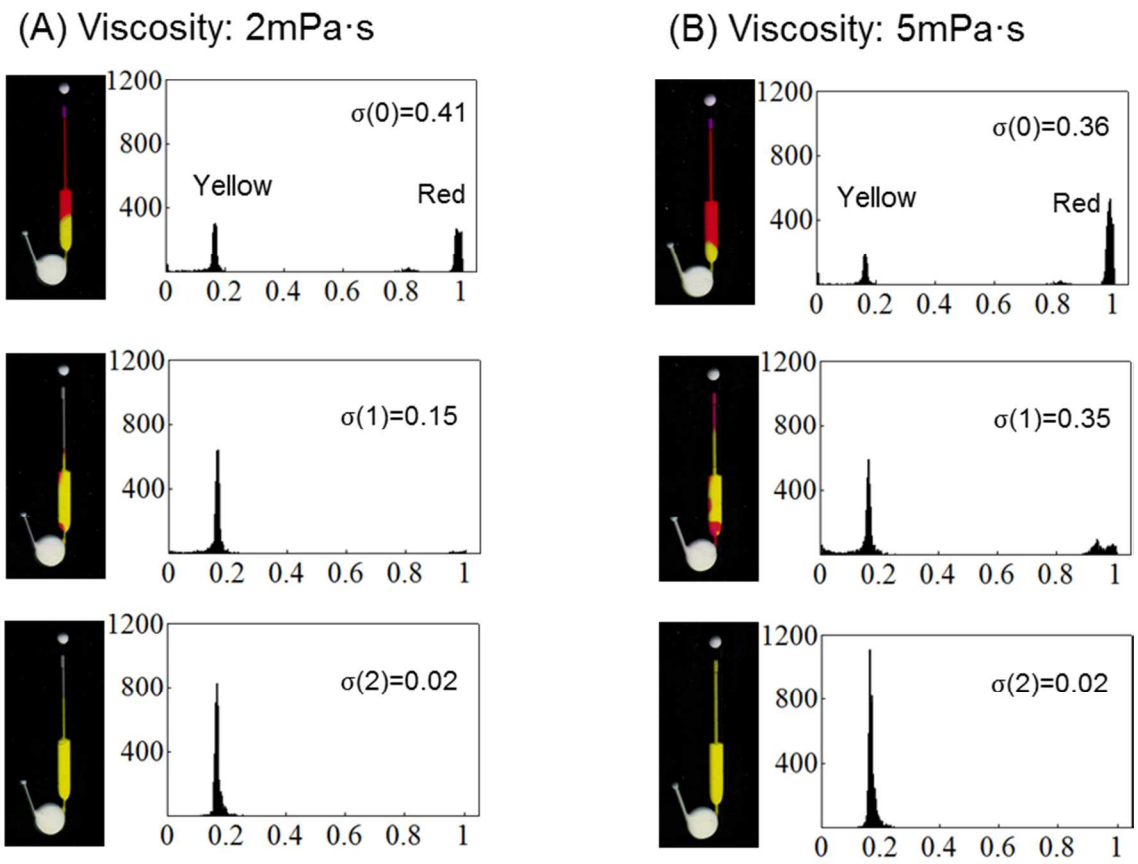

Fig.4: Representative snapshots of the dye distribution in the mixing unit as the number of the reciprocating cycle increases (n=3) when viscosity is (A) 2 mPa·s and (B) 5 mPa·s. Evaluation of the mixing process was done by analyzing the distribution of dye pixel intensities in the histogram as a function of reciprocating cycle number.

In designing the domain containing the aliquoting chamber, toner valves and the waste chamber, several critical design and fabrication considerations played into the accuracy of the metering method, including: (1) minimizing alignment error with multiple Pe layers; (2) the break-off process involving an air plug displacing the liquid in the distribution channel during overflow at the intersection of the distribution channel and the aliquot chamber inlet (**Figure** 1B).

The aliquot volume is geometrically defined as the region between the intersection of the aliquot chamber with the feeding channel and the hydrophobic toner barrier at the end of the chamber, hence, minimizing the misalignment of the hydrophobic barriers (both ceiling and floor of the channel) is essential. We addressed this by designing an alignment port that is laser cut in each layer for simple assembly using an alignment pin; this assures alignment precision with a tolerance of up to ~500 µm. In addition, all of the hydrophobic valves connected to aliquoting chambers have a width of 300 µm which is determined by the minimum attainable channel width via laser ablation for constructing a reliable hydrophobic valve on PeT microchip[10]. Therefore, longitudinal misalignment of the toner patches on the top and bottom of the channel can result in an uncertainty in volume of ~20 nL ($w \times l \times d$ = 300 µm × 500 µm × 132 µm). As a result, the effect on precision/accuracy of the aliquoted volumes will range over roughly an order of magnitude, depending on the volume aliquoted. With a 2.25 µL chamber, the error is negligible, however, with a 250 nL chamber volume, error from misalignment is expected to be ~8%, which mirrors that obtained with an conventional micropipetting[13].

In addition to multi-layer alignment, reliable and precise aliquoting is specifically impacted by the 'break-off' process (occurs when an air plug displaces the liquid in the feed channel during the overflow process) cut at the intersection of the distributing channel with the inlet of the aliquot chamber (**Figure** 1B). The design shown in Fig.1B addressed two issues that negatively impact successful aliquoting of desired volumes. One design feature is the use of multiple air vents connected to the feeding channel. The placement of an air vent connecting the feeding channel to each aliquot chamber is to counteract an undesirable siphoning effect with the first spinning step shown in

Figure 2B. On the rotating disk, the siphoning effect can be observed as a series of continuous liquid plug possessing different artificial gravitational potentials; this has been discussed in detail in a couple of review articles [14,15]. In the absence of this feature, as long as the nearest aliquot chamber is still fluidically-connected to the waste chamber, undesirable siphoning from the aliquot chamber to the waste chamber could occur. As a result, the aliquot chamber could only be partially filled. In contrast, by adding multiple air vents to the design, this modification facilitates the creation of air plugs in the feeding channel to displace fluid flowing to the waste channels, thus, preventing the siphoning effect. Another feature of the design is that, the feeding channel consists of repeated "V" structure units rather than using an arc-shape (**Figure** 1B). The upper point of the aliquot chambers is placed at the top part of 'V' structure, being closer to the center of the chip, while the upper point of waste channel is placed on the bottom tip of the 'V' structure. Each waste channel is separated from the air vents by a half segment of the 'V' channel. If any small residue is generated in the feeding channel during the first spinning step shown in **Figure** 3B, it can be favorably guided to the waste chamber later.

Reciprocating mixing performance

Figure 4 illustrates the efficacy of the reciprocating mixing strategy described earlier in the *Overview Section*. In this study, the test device is simplified to include only one reciprocating mixer which have two fluidic layers for the addition of two solutions. To visualize the mixing, we used two dye solutions of different colors - yellow (tartrazine in 0.1 M HCl) and magenta (phenolphthalein in 0.08 M NaOH). As the yellow and magenta solutions were loaded to fluidic layers physically-separated by the third layer, areas of the dye solutions overlapped visually presented as a red color. From a chemical perspective, complete mixing of the dyes creates an acidic pH, resulting the magenta color of phenolphthalein fading. Thus, as mixing progresses to completion, the solution color should eventually turn into yellow.

Since the final aliquot rotation speed is 1200 rpm, centrifugal pumping of the solutions into the cylindrical chamber (Fig. 1) was at 1200 rpm for 15 sec, which was more than sufficient to counteract the surface tension. The backflow time was experimentally determined to be 5 sec at 0 rpm. In **Figure** 4, optical images of the reciprocating mixer, showing red and yellow fluids, is presented next to the corresponding histogram profiles of the fluid after mixing by spin oscillation. We quantitated the extent of mixing through 'hue profiles' from images of the chip chamber prior to and following every reciprocating mixing cycle. Only pixels representing the mixture were transferred into a normalized hue histogram to calculate the standard deviation $\boldsymbol{\sigma(n)}$ for evaluating the mixing efficiency [16]. In **Figure** 4, we show the evolution of $\boldsymbol{\sigma(n)}$, the standard deviation of the histogram distribution, during the reciprocating mixing cycles of two solutions varying in viscosity[17]: dyes in 25% (wt/wt) glycerol (a ~2 mPa·s viscosity, comparable to that of human blood serum) (Fig. 4A) and dyes in 45% (wt/wt) glycerol (a ~5 mPa·s viscosity, comparable to that of whole blood) (Fig. 4B). A decrease in $\boldsymbol{\sigma(n)}$ was clearly observed as the number of reciprocating cycles increased. After two cycles, the histograms from both solutions began to follow a Gaussian distribution, and displayed a hue histogram that correlated with that from homogenously mixed dyes, (i.e., comparable to a mixture prepared by pipetting and vortexing in an Eppendorf tube).

A number of approaches were utilized in the early implementation of mixing units by many research groups[16,18–20], and the majority of them have been reviewed in detail by Gorkin et.al[21]. Among these, the reciprocating mixing unit reported by Noroozi et al.[20], exploits the same 'spin and stop' actuation that we describe here, however, it relies on the pneumatic agitation energy. In that method, a stream of compressed gas was generated when the disc was span at 7000 rpm, and then released when the spinning was paused, during which the liquid could be reciprocated between two domains, ultimately enhancing mixing. This 'air agitation' approach can be broadly applied to microfluidic devices as a result of there being little dependence on surface characteristics. In contrast to this approach, our mixing design takes advantage of the spontaneous capillary action derived from the native hydrophilic property of the Pe film surface and, most importantly, requires relatively low operational spin speeds for mixing (1200 rpm). In addition, the PeT device here weighs less than 60% of a traditional music CD disk and, thus, requires a lower torque to spin at a particular rotation speed than that of a traditional CD disc. A 6-fold decrease in rotation speed and the lower torque requirement moves us into a regime that allows for flow to, indeed, be driven by a CD player. A lower rpm and torque approach has a lower power consumption, providing the potential for inexpensive hardware associated with handheld CD-players to be used. This has obvious ramifications on the hardware cost reduction and the enhancement of portability.

In the development of the reciprocating mixer shown in **Figure** 1, geometrical considerations were addressed to facilitate and enhance the mixing process, while being cognizant of space usage efficiency. The mixing units were comprised of a pair of identical split detection channels that overlapped with each other, and a cylindrical mixing chamber. The basic idea behind this is that the reciprocating mixer allows the two solutions to repeatedly split and recombine during the oscillation spins. In one aspect, the principle is similar to the 'serial laminated mixers' reviewed by Nguyen et.al[22]. To best simplify the detection channel design and increase the space usage efficiency, the detection channel width (3 mm) is designed to be much larger than the chamber depth (~ 132 μm). According to the Young-Laplace equation, the capillarity of the detection channel is dominated by the channel depth, which is determined here by the thickness of the Pe and toner layers. As such, the backflow velocity is mainly determined by the depth of the detection channel. The volume of the mixing chamber was designed to be the same as that of the aliquot mixture, thus, reducing the flow path length for the mixture between the mixing chamber and the split detection channels. Another noteworthy aspect of the design is the cylindrical shape of the mixing chamber, which has been proven beneficial in promoting advective fluidic currents to enhance mixing during the rotation acceleration and deceleration[16].

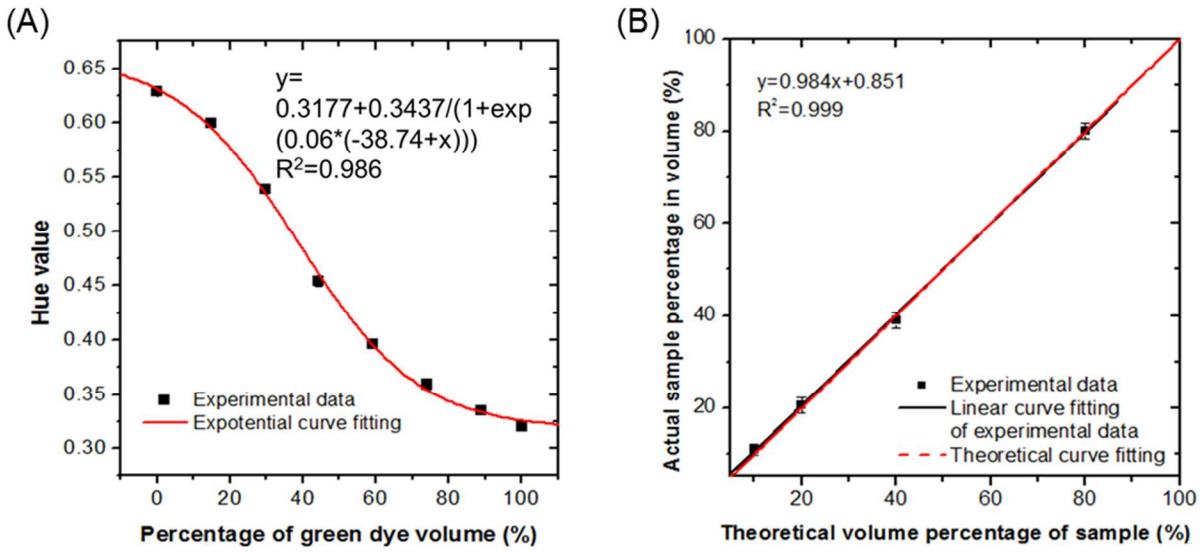

Fig.5: Validation of the dilution performance by loading the blue and green dyes to the microchip to mimic the sample reagent and buffer reagent, respectively. (A) The calibration curve correlating the mean intensity of the hue in the detection zone of the microchip with the percentage of $V_{\text{Green Dye}}$ / [$V_{\text{Green Dye}}$ +$V_{\text{Blue Dye}}$] (n=4). (B) Comparison of the empirical dilution with the calculated dilution on the PeT microchip (n=4).

Dilution performance by integration of metering and mixing functionality

Once all of the individual metering and mixing features were designed and optimized, these were combined into a single chip for parallel dilution. The dilution performance was quantified by diluting a green dye solution (mock sample) with a blue dye solution (mock buffer) on chip, employing the operation steps in **Figure** 2 with three reciprocating mixing cycles. We quantified the amount of each dye presented in the final solution using spectroscopy (a scanner and a custom-built image algorithm). **Figure** 5A shows the calibration curve that relates the hue value obtained from processing optical images as a function of percentage of sample volume in the final solution. This calibration curve was used to calculate the final 'sample content' in a mixed volume following the reciprocating spin cycles described earlier. **Figure** 5B illustrates near-perfect agreement between the expected and the measured sample concentrations obtained on chip. This confirms the feasibility of simultaneous, parallel aliquoting of sample and buffer into different fluidic levels of the microchannel architecture, and substantiates that effective mixing can be achieved on this five-layer PeT microchip.

Colorimetric protein assay

Various blood tests have been demonstrated on many other types of microfluidic discs [23–28]. As a proof of concept, the final design for our microfluidic disc was tested for quantifying the total protein concentration in blood plasma. The protein level in the blood can be an indicator of health status with the normal total serum protein concentration in a healthy adult ranging from 60-83 mg/mL[11]. Levels outside this concentration range can be indicative of numerous pathologies including kidney disease, liver disease, hyperthyroidism and blood diseases or immune system problems[29].

First, a calibration curve for the protein assay was generated by pipetting 2.5 µL of artificial human blood plasma (containing different human serum albumin (HSA) concentrations) and 2.5 µL of tetrabromophenol blue (TBPB) solution to the mixing domain. After completing the colorimetric detection of total protein in the artificial human blood plasma by a scanner, the area of each detection chamber in the image was 'cropped' in Image J to measure the average hue. With the calibration curve shown in **Figure** 6A, the limit of detection (LOD) was calculated based on three times of the standard deviation of the hue value read from the mock sample without addition of HSA. The LOD was determined to be ~5 mg/mL, clearly well below the lower end of the normal range. Increasing the protein concentration from 0 mg/mL to 80 mg/mL resulted in sufficient increases in the hue value. It is clear that this colorimetric chemistry can differentiate a clinically-relevant low protein concentration (45 mg/mL) from the lower normal limit of the normal range (60 mg/mL). However, the plateauing between 80 and 100 mg/mL suggests that the assay is less sensitive to higher protein levels (hue values at 70 mg/mL, 80 mg/mL and 90 mg/mL were 0.515, 0.532 and 0.542, respectively, with S.D. varying from ±0.004 to ±0.006). Therefore, samples with a protein concentration greater than 80 mg/mL require dilution for accurate quantitation.

The PCL microfluidic disc was tested on the quantitation of total protein both in the mock samples of human blood plasma (artificial human blood plasma spiked with HSA used for calibration) and unknown human lithium-heparin plasma samples obtained from a hospital clinical lab. The sample of interest was loaded into the sample metering layer, while the buffer solution (artificial human blood plasma buffer without HSA) was loaded into the buffer metering layer. After completion of step A-C shown in **Figure** 2, 2.5 µL of TBPB indicator was pipetted through the reservoir connected to the detection chamber of each

Cite this: DOI: 10.1039/c0xx00000x

www.rsc.org/xxxxxx

ARTICLE TYPE

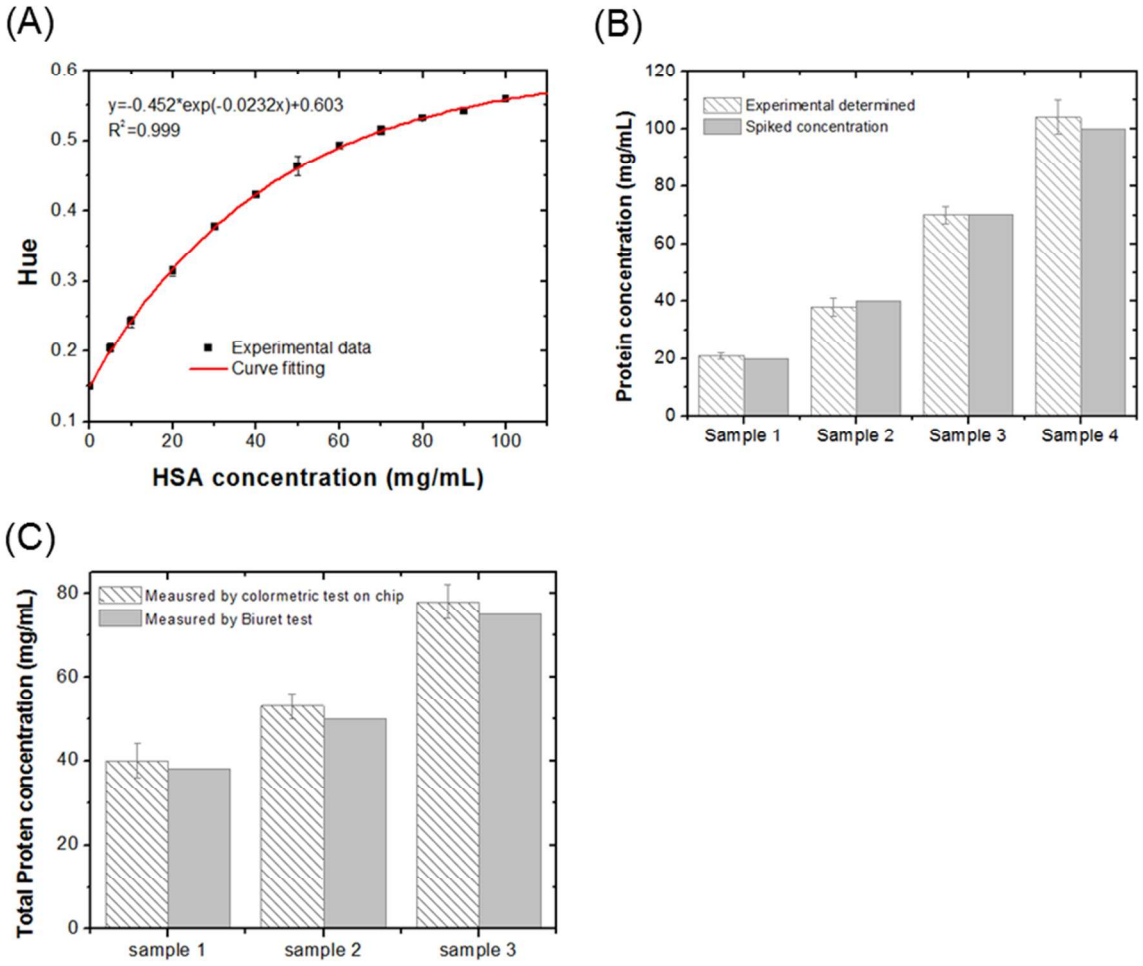

Fig.6: Result of the protein quantitation on chip. (A)The calibration curve for the quantitation of total protein concentration in the artificial human blood plasma. Result of the protein quantitation for (B) mock samples and (C) real sample of human blood plasma on PeT microchip (n=3).

micromixer domain, and reciprocating mixing was initiated following steps D-E. The entire process, from loading to the final hue-based detection, required less than 10 min. When the averaged hue values for each mixing chamber were plugged into the calibration curve, the post-dilution protein concentration ($\boldsymbol{C_i}$) was generated. If the hue value was outside the calibration curve dynamic range, that result was excluded in the final calculation. The original protein concentration in the mock samples ($\boldsymbol{C_{protein}}$) was calculated from Eq (1), expressed as follow:

$$C_{protein} = \frac{1}{n}\sum_1^n C_i \times k_i \qquad (1)$$

where k_i represents the particular dilution ratio (e.g., 10, 5, 2.5 and 1.25 for the chip design in Fig. 1C) in that specific micromixer domain.

As seen in **Figure** 6B which compares with spiked concentrations with the measured values, the device is highly effective in achieving a broad range of protein concentrations for subsequent analysis. **Figure** 6C shows the average values for protein concentration determined by the PCL microfluidic disc for clinical plasma samples are slightly higher than the concentrations determined by a modified biuret test carried out by Abbott Architect c16000 analyzer in a Clinical Chemistry Lab at University of Virginia. The discrepancy likely emanates from the use of a single calibrate protein (HSA) to generate the on-chip calibration curve, which is unlikely to represent the very diverse array of proteins present in blood. In contrast, the commercial modified biuret system utilizes a commercial reagent kit that more accurately represents the blood proteins for standard calibration. Nevertheless, the PeT disc demonstrated a satisfactory fluidic processing for clinically-relevant samples.

Conclusions

For the first time, we show the design, fabrication and functionalization of an intricate, 3D microfluidic architecture in a

five-layer PCL microfluidic disc in PeT with two fluidic levels using a simple fabrication procedure. The open fluidic architecture, passive valving/mixing functions, and ability to laser print valves during fabrication are all attractive features. Unique to the design is the multi-level microfluidic configuration which enables aliquoting and simultaneous dilution in the nL to µL range with effective mixing manner for samples with biologically-relevant viscosities. Driven by centrifugal force, both valving actuation and mixing are rotation speed controlled, requiring no more than a battery-powered CD-player with rotation speeds achievable by a handheld player. Detection is colorimetric, utilizing a $100 desktop scanner to determine hue which, against a calibration curve, allowed for demonstration of a protein quantitation assay. It compares favorably with paper-based microfluidics, both in simplicity and cost-effectiveness, but outperforms paper systems with better precision, faster analysis time (3-fold)[11]. Although the cost for low rate manufacture (in our lab) is <$2 per device which is slightly more expensive than the paperfluidic devices, upon mass production, it could potentially be decreased by an order of magnitude. An additional noteworthy point is that the dispensing technologies used for lateral flow strip manufacturing[30] could also be used on PCL microfluidic discs. Combining with the dried, on-chip stored reagent technologies[31–33], the PCL microfluidic disc could be improved as a self-contained cartridge while the incremental increase in fabrication cost would be insignificant.

The paradigm of the fluidic control and detection outlined this paper represents a step toward an integrated, portable PCL microfluidic disc, one that eliminates error-prone manual steps and reduces the human exposure to reagents with rapid 'sample-to-result' capabilities. The versatility of the PeT microchip can be further enhanced by implementing some existing technologies that have been turned into flexible modules by other researchers[34–37]. For example, the use of siphoning valve[37] will enable separation of liquid (i.e., plasma) from particles (i.e., blood cell) at first high RPM spinning step, so that the PCL microfluidic disc can directly handle samples with higher complexity (i.e., crude blood samples). We are also working on enhancing portability of the ancillary hardware, that is substituting the desk scanner by a smart phone with image processing functionality, and integrating the detection unit to a reengineered CD player to create a fully-portable system. The combination of all above efforts will ultimately allow easy adaption of many different kinds of biological assays on one PCL microfluidic disc for multiplexed point-of-care analysis.

Acknowledgements

The authors (James P. Landers and Matthew R. Begley) express gratitude to the NIH for support on exploration of passive valving approaches for microfluidic systems (NIH R01 KK1103). Support from the Ivy Biomedical Innovation Fund is also gratefully acknowledged by James P. Landers.

Notes and references

[a]*Department of Chemistry, McCormick Road, University of Virginia, Charlottesville, VA 22904*
[b]*Mechanical Engineering, 315 Ferst Drive, Georgia Institute of Technology, Atlanta, GA 30332-0363*
[c]*Department of Mechanical Engineering & Materials Department, University of California Santa Barbara, Santa Barbara, CA, 93106Address here.*
[d]*Department of Pathology, University of Virginia Health Science Center, Charlottesville, VA 22908*
[e]*Department of Mechanical Engineering, University of Virginia, Engineer's Way, Charlottesville, VA 22904*

1. X. Li, D. R. Ballerini, and W. Shen, *Biomicrofluidics*, 2012, **6**, 11301–1130113.
2. P. Lisowski and P. K. Zarzycki, *Chromatographia*, 2013, **76**, 1201–1214.
3. A. W. Martinez, S. T. Phillips, M. J. Butte, and G. M. Whitesides, *Angew. Chem. Int. Ed. Engl.*, 2007, **46**, 1318–20.
4. A. W. Martinez, S. T. Phillips, E. Carrilho, S. W. Thomas, H. Sindi, and G. M. Whitesides, *Anal. Chem.*, 2008, **80**, 3699–707.
5. S. J. Vella, P. Beattie, R. Cademartiri, A. Laromaine, A. W. Martinez, S. T. Phillips, K. a Mirica, and G. M. Whitesides, *Anal. Chem.*, 2012, **84**, 2883–91.
6. A. V Govindarajan, S. Ramachandran, G. D. Vigil, and P. Yager, 2012, 174–181.
7. J. Tian, D. Kannangara, X. Li, and W. Shen, *Lab Chip*, 2010, **10**, 2258–64.
8. C. L. do Lago, H. D. T. da Silva, C. A. Neves, J. G. A. Brito-Neto, and J. A. F. da Silva, *Anal. Chem.*, 2003, **75**, 3853–8.
9. G. R. M. Duarte, C. W. Price, B. H. Augustine, E. Carrilho, and J. P. Landers, *Anal. Chem.*, 2011, 5182–5189.
10. Y. Ouyang, S. Wang, J. Li, P. S. Riehl, M. Begley, and J. P. Landers, *Lab Chip*, 2013, 1762–1771.
11. S. J. Vella, P. Beattie, R. Cademartiri, A. Laromaine, A. W. Martinez, S. T. Phillips, K. A. Mirica, and G. M. Whitesides, *Anal. Chem.*, 2012, **84**, 2883–91.
12. L. Liu, C. L. Qiu, Q. Chen, and S. M. Zhang, 2006, **425**, 268–273.
13. www.eppendorf.com/int/index.php?pb=d619ab0aa3358bb
14. J. Ducrée, S. Haeberle, S. Lutz, S. Pausch, F. Von Stetten, and R. Zengerle, *J. Micromechanics Microengineering*, 2007, **17**, S103–S115.
15. R. Gorkin, J. Park, J. Siegrist, M. Amasia, B. S. Lee, J.-M. Park, J. Kim, H. Kim, M. Madou, and Y.-K. Cho, *Lab Chip*, 2010, 1758–1773.
16. M. Grumann, a Geipel, L. Riegger, R. Zengerle, and J. Ducrée, *Lab Chip*, 2005, **5**, 560–5.

17. P. Garstecki, M. J Fuerstman, M. a Fischbach, S. K. Sia, and G. M. Whitesides, *Lab Chip*, 2006, **6**, 207–12.

18. S. Haeberle, T. Brenner, H.-P. Schlosser, R. Zengerle, and J. Ducrée, *Chem. Eng. Technol.*, 2005, **28**, 613–616.

19. M. Kong and E. Salin, *Microfluid. Nanofluidics*, 2012, **13**, 519–525.

20. H. Noroozi, Zahra, Kido, R. J. Peytavi, Régis Nakajima-sasaki, and et al Algimantas Jasinskas, Miodrag Micic, Philip L.Felgner, Marc J. Madou, *Review of Scientific Instruments* 2012, **064303**.

21. R. Gorkin, J. Park, J. Siegrist, M. Amasia, S. Lee, J. Park, J. Kim, H. Kim, and Y. Cho, 2010, 1758–1773.

22. N.-T. Nguyen and Z. Wu, *J. Micromechanics Microengineering*, 2005, **15**, R1–R16.

23. J. Steigert, T. Brenner, M. Grumann, L. Riegger, S. Lutz, R. Zengerle, and J. Ducrée, *Biomed. Microdevices*, 2007, **9**, 675–9.

24. M. Grumann, J. Steigert, L. Riegger, I. Moser, B. Enderle, K. Riebeseel, G. Urban, R. Zengerle, and J. Ducrée, *Biomed. Microdevices*, 2006, **8**, 209–14.

25. R. Gorkin, J. Park, J. Siegrist, M. Amasia, B. S. Lee, J.-M. Park, J. Kim, H. Kim, M. Madou, and Y.-K. Cho, *Lab Chip*, 2010, **10**, 1758–73.

26. Y.-K. Cho, J.-G. Lee, J.-M. Park, B.-S. Lee, Y. Lee, and C. Ko, *Lab Chip*, 2007, **7**, 565–73.

27. J. Park, V. Sunkara, T.-H. Kim, H. Hwang, and Y.-K. Cho, *Anal. Chem.*, 2012, **84**, 2133–40.

28. D. J. Kinahan, M. T. Glynn, S. M. Kearney, and J. Ducrée, 2012, 1363–1365.

29. http://www.webmd.com/a-to-z-guides/total-serum-protein?page=2

30. B. O. Farrell, *The immunoassay handbook*, Elsevier Ltd, Fourth Edi., 2013.

31. B. S. Lee, Y. U. Lee, H.-S. Kim, T.-H. Kim, J. Park, J.-G. Lee, J. Kim, H. Kim, W. G. Lee, and Y.-K. Cho, *Lab Chip*, 2011, **11**, 70–8.

32. R. Z. and F. von S. J.Hoffymaan, D. Mark, in *Transducers*, 2009, pp. 1991–1994.

33. M. Focke, F. Stumpf, B. Faltin, P. Reith, D. Bamarni, S. Wadle, C. Müller, H. Reinecke, J. Schrenzel, P. Francois, D. Mark, G. Roth, R. Zengerle, and F. von Stetten, *Lab Chip*, 2010, **10**, 2519–26.

34. Y. Sun, J. Høgberg, T. Christine, L. Florian, L. G. Monsalve, S. Rodriguez, C. Cao, A. Wolff, J. M. Ruano-Lopez, and D. D. Bang, *Lab Chip*, 2013, **13**, 1509–14.

35. S. Wang, X. Zhao, I. Khimji, R. Akbas, W. Qiu, D. Edwards, D. W. Cramer, B. Ye, and U. Demirci, *Lab Chip*, 2011, **11**, 3411–8.

36. H. Zhu, O. Yaglidere, T.-W. Su, D. Tseng, and A. Ozcan, *Lab Chip*, 2011, **11**, 315–22.

37. J. Steigert, T. Brenner, M. Grumann, L. Riegger, S. Lutz, R. Zengerle, and J. Ducrée, *Biomed. Microdevices*, 2007, **9**, 675–9.